

# **A one-dimensional mixing model to investigate the impact of Ablative Rayleigh-Taylor Instability on compression**

Dongxue Liu,<sup>1</sup> Tao Tao,<sup>1</sup> Jun Li<sup>1,3</sup>, Qing Jia<sup>1</sup>, Rui Yan<sup>2,3</sup>, and Jian Zheng<sup>1,3,\*</sup>

- 1 (Department of Plasma Physics and Fusion Engineering, University of Science and Technology of China, Hefei 230026, People's Republic of China)
- 2 (Department of Modern Mechanics, University of Science and Technology of China, Hefei 230027, People's Republic of China)
- 3 (Collaborative Innovation Center of IFSA, Shanghai Jiao Tong University, Shanghai, 200240, People's Republic of China)

Email: [jzheng@ustc.edu.cn](mailto:jzheng@ustc.edu.cn)

## **Abstract**

We propose a one-dimensional mixing model to investigate the impact of Ablative Rayleigh-Taylor Instability (ARTI) on compression, addressing the limitations of high-dimensional simulations. In this model, the scale of the mixed region is predicted using an ablative buoyancy drag model and the mass-weighted average field distributions in the direction of acceleration are obtained by interpolating between the initial and final isothermal molecule mixing states based on the mixing extent, defined by the percentage of maximum specific turbulent kinetic energy and a free multiplier  $f$ , which varies from chunk mixing (0) to atomic mixing (1). After validation through two-dimensional simulations, the model is integrated into a Lagrangian framework and applied to spherical implosion scenarios. The results indicate that the compression of

the inflight shell is diminished, leading to a reduced time interval between the convergence of the main shock and stagnation, potentially providing a measurable signal in single-shot experiments.

**Keywords:** mixing model, compression, isothermal molecular mixing

## I. Introduction

Laboratory fusion ignition [1, 2] has been successfully achieved at the National Ignition Facility (NIF) using a central ignition scheme, where low-density deuterium-tritium (DT) gas is compressed and heated by a surrounding cold DT fuel layer, leading to the formation of a hot spot. The hot spot is self-heated by  $\alpha$  particles, facilitating the propagation of a burn wave [3]. Both the quality of the hot spot and the effectiveness of self-heating, are closely linked to the compression dynamics [4, 5]. Numerous experiments [6-14] have observed reduced compression, quantified by parameters such as adiabat, areal density and inflight shell thickness. Therefore, researchers have investigated the physical mechanisms underlying the observed deficiencies in compression throughout various phases of implosions.

Hydrodynamic instabilities across various scales contribute to the reduced compression. Low-mode drive asymmetry [15, 16], arising from hohlraum geometry or cross-beam energy transfer (CBET) [17, 18], leads to asymmetric compression and diminished fuel compression at stagnation. In addition to preheating [19-22], high-mode non-uniformities at the fuel-ablator interface [23, 24] can increase fuel entropy through mixing processes. Furthermore, Ablative Rayleigh-Taylor Instability (ARTI), seeded by target defects [25, 26] and laser imprint [27, 28], compromises compression

prior to the onset of these instabilities.

To address the computational challenges of high-precision two-dimensional (2D) and three-dimensional (3D) simulations [29, 30], approaches of rapid and adjustable one-dimensional (1D) simulations have been employed. For instance, the fall-line mix model [31] modifies the fusion process using a free multiplier to adjust the width of the fully atomized mixed region during the deceleration phase. Similarly, field distributions within the mixed region, refined by the buoyancy-drag (BD) model [32, 33] at the CH-DT interface, are modified by the extent of mixing through a free multiplier known as surface-to-volume (AOV). Furthermore, the 1D Reynolds-averaged Navier-Stokes [34, 35] equations describe the distribution of average fields by applying coefficients suitable for turbulent phases. However, these mixing models are not directly applicable to ARTI.

In this paper, we propose a 1D mixing model within the mixed region, refined by an ablative BD [36, 37] model, to describe the impact of ARTI on compression. This model modifies the mass-weighted average fields in the direction of acceleration by interpolating between initial and final isothermal molecule mixing states, based on the extent of mixing. This extent is a function of the percentage of maximum specific turbulent kinetic energy  $K_{f0}$  and a free multiplier  $f$ , ranging from chunk mixing (0) to atomic mixing (1). Upon validation through simulations and successful implementation in a Lagrangian framework, this model provides a valuable tool for evaluating the impact of reduced compression on the quality of spherical implosion.

The paper is arranged as follows. We first elaborate the 1D mixing model based on

simulations in Section II. In section III, we implement the 1D mixing model into MULTI-IFE [39] and compare its results with FLASH [38] simulations. Following these validations, the impact of the 1D mixing model on spherical implosions is examined in section IV. Finally, we draw our conclusions in section V.

## II. 1D mixing model based on simulations

In ICF, high-mode nonlinear ARTI induces the mixing of hot and cold fluids. Based on the mixing characteristics revealed through simulations, we propose a 1D mixing model to efficiently analyze the effect of mixing on the spatially averaged fields.

We first illustrate the changes in field distributions resulting from velocity perturbations  $V_p(\mathbf{x})$ , simulated using FLASH [37]. As shown in Fig. 1, the mixed region is located between the bubble front and the spike front. The white ellipses highlight prominent bubbles, where  $V_p(\mathbf{x})$  in the  $X$  direction causes significant density fluctuations. These negative density fluctuations lead to substantial positive pressure variations due to the differing distances between the critical density front and the ablation front, as depicted in Fig. 1(c). Consequently, these pressure variations induce considerable velocity perturbations in the  $Y$  direction, as shown in Fig. 1(d), further stimulating density fluctuations and contributing to the formation of bubble and spike structures shown in Fig. 1(a). These nonlinear structures emerge from the interpenetration between hot, low-density plasma and cold, dense plasma, leading to a negative correlation between fluctuations in electron specific internal energy  $e_e$  and density fluctuations as demonstrated in Fig. 1(b) and (a). It is noteworthy that pressure perturbations may not increase with decreasing density fluctuations on a small scale

due to the influence of electron heat conduction.

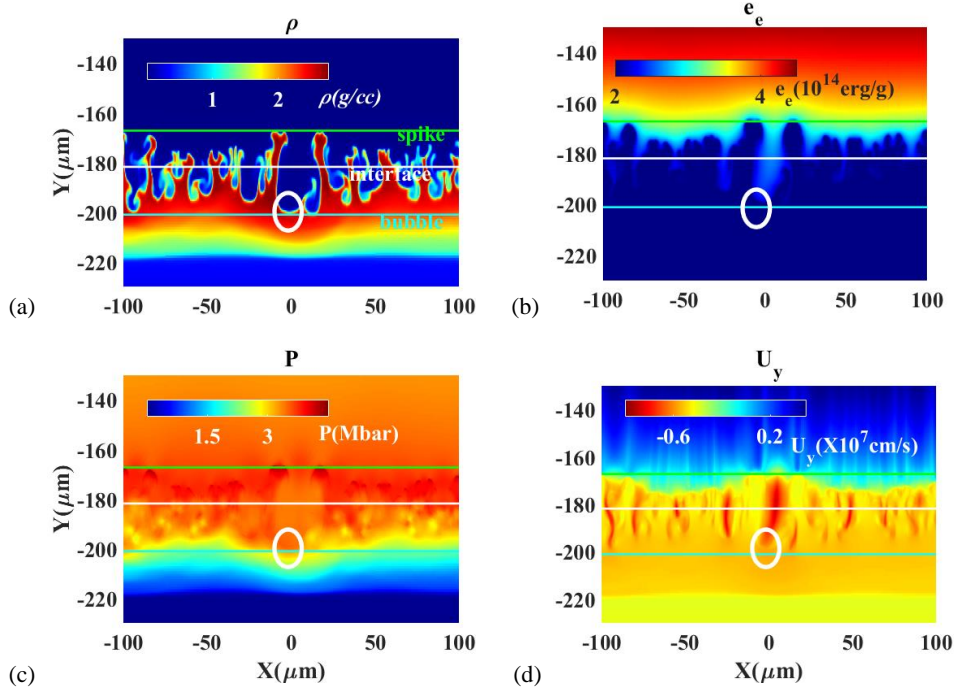


Fig. 1. Distribution of (a) density  $\rho$ , (b)  $e_e$ , (c) pressure  $P$  and (d) velocity  $U_y$ , where the white

ellipses represent large bubbles. The simulation settings are as follows: the lengths of the simulation domain

in the  $X$  and  $Y$  directions are denoted as  $L_x = [-100\mu m, 100\mu m]$  and

$L_y = [-400\mu m, 2000\mu m]$ , with a spatial resolution of  $0.52 \mu m$ . The vertically irradiated laser

pulse, is square-shaped with a rise time of  $0.1 \text{ ns}$  and a peak intensity of  $25 \text{ TW} / \text{cm}^2$ . The CH planar

target has a density of  $1 \text{ g} / \text{cc}$  and a thickness of  $90 \mu m$ . The multi-mode velocity perturbations,

introduced as seeding sources adjacent to the surface, are defined as

$$V_p(x) = \sum V_{pk} \cos mk_L x + \psi_{k0}, \quad k_L = 2\pi / L_x, \text{ where } m \text{ is an integer ranging from 4 to 10,}$$

$\psi_{k0}$  is a random phase uniformly distributed between zero and one,  $V_{pk} = V_p k_0 e^{(-mk_L |y - y_0|)}$ ,

$V_{pk0} = C mk_L^{-2}$ , and  $C$  is a constant.

Fig. 2 presents a detailed analysis of the field illustrated in Fig. 1(b) through spatial average, indicating that mixing results in an increase in the characteristic scale of the ablation front, transitioning from initial state without mixing  $\tilde{e}_{e,ini}$  to a mixing state  $\tilde{e}_{e,mid}$ . This observation motivates the development of a 1D mixing model to

investigate the 1D spatially averaged fields. The forcing equation,

$$\frac{\partial \langle \rho \rangle \tilde{U}_j}{\partial t} + \frac{\partial \langle \rho \rangle \tilde{U}_j \tilde{U}_j}{\partial x_j} = - \frac{\partial \langle P \rangle}{\partial x_j} - \frac{\partial \langle \rho U_j'' U_j'' \rangle}{\partial x_j},$$

incorporates both spatial average  $\rho = \langle \rho \rangle + \rho'$  and mass-weighted average

$$U = \tilde{U} + U'', \text{ where } \tilde{U} = \frac{\langle \rho U \rangle}{\langle \rho \rangle} = \langle U \rangle + \frac{\langle \rho' U' \rangle}{\langle \rho \rangle}, \langle \rho \rangle, \rho', \tilde{U} \text{ and } U''$$

represent the mean and fluctuated density of spatial average, the mean and fluctuated velocity of mass-weighted spatial average, respectively. The right-hand side of this equation comprises two main components: hot pressure  $P$  and shear force related to velocity gradient. Given that the pressure gradient exceeds the velocity gradient near the ablation front, we conclude that hot pressure, intrinsically dependent on  $\rho$  and specific internal energy  $e$ , is the dominant force contributing to mixing.

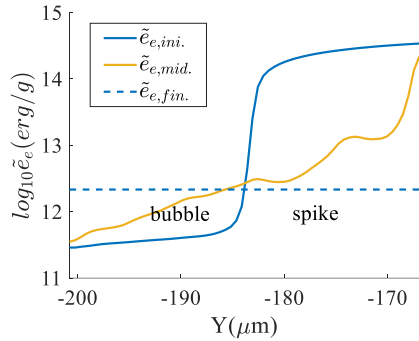


Fig. 2 Distributions of  $\tilde{e}_e$  in the initial state  $\tilde{e}_{e,ini}$ , the middle state  $\tilde{e}_{e,mid}$  calculated from Fig. 1(b)

and the final state of isothermal mixing  $\tilde{e}_{e,fin}$ .  $\int_Y \langle \rho \rangle \tilde{e}_{e,ini} dY = \int_Y \langle \rho \rangle \tilde{e}_{e,fin} dY$  The minor difference between  $\tilde{e}_{e,ini}$  and  $\tilde{e}_{e,fin}$  within the bubble region supports modifying  $\tilde{e}_e$  through interpolating between the initial and final states.

In Fig. 2,  $\tilde{e}_{e,mid}$  at the spike front and the bubble front are nearly identical to  $\tilde{e}_{e,ini}$ , indicating that the mixed region is the primary area influenced. The final isothermal molecular mixing state, represented as  $\tilde{e}_{e,fin}$  in Fig. 2(a), can be achieved

as the mean perturbation wavelength decreases with the increasing mixed region. The distribution of  $\tilde{e}_{e,mid}$  and the minor difference between  $\tilde{e}_{e,ini.}$  and  $\tilde{e}_{e,fin.}$  support our approach of modifying  $\tilde{e}_e$  by interpolating between the initial and final states based on the extent of mixing.

The mixed region is refined utilizing the BD model, which also provides the bubble velocity  $v_B$  necessary for calculating  $K_{f0} = \frac{1}{2}v_B^2$ . The specific turbulent kinetic energy  $K_f$  at the interface of bubbles and spikes can reach its maximum  $K_{f0}$  if the average perturbation wavelength is sufficiently small to achieve an isothermal molecule mixing state, otherwise it remains smaller than  $K_{f0}$ . Therefore,  $K_f$  within the mixed region, similar to that in RANS model [34], can be expressed as  $K_f = fK_{f0}(1 - y^2/h_B^2)$ , where  $f$  is a constant representing the ratio of mean perturbation wavelength at the point of isothermal molecule mixing to the current mean perturbation wavelength, with a range from chunk mixing (0) to atomic mixing (1), and  $h_B$  denotes the bubble penetration distance. Using  $\tilde{E}_k$  to represent total kinetic energy of unit mass, the extent of mixing, denoted as  $ME$ , is characterized as time varying through  $K_f / \tilde{E}_k$ , which approaches 0 in the absence of mixing, while in a state of isothermal molecule mixing, it approaches a constant value not greater than 1. Consequently, the expression for the modified term of  $\tilde{e}_e$  is given by:

$$\tilde{e}_{e,1Dmixng} = e_{e,1D} + \Delta\tilde{e}_e ME, \quad (1)$$

where  $ME = \sqrt{K_f / \tilde{E}_k}$  pertains to the bubble region,  $ME = \sqrt{K_f / \tilde{E}_k} \cdot \xi$

pertains to the spike region,  $\xi = \left| \frac{\int_{V \in bubble} \Delta \tilde{e}_e \cdot \sqrt{K_f / \tilde{E}_k} \rho dV}{\int_{V \in spike} \Delta \tilde{e}_e \cdot \sqrt{K_f / \tilde{E}_k} \rho dV} \right|$  is employed to

ensure energy conservation within the mixing zone, and  $V$  represents the volume of each computational cell in various geometries. In the mixed region, thermal relaxation facilitates the equilibration of temperatures between electrons and ions, resulting in an analogous 1D mixing model for the mass weighted spatially averaged specific internal energy of ions. Consequently, we implement the 1D mixing model into MULTI-IFE prior to the equation of state (EOS) lookup, which is executed once per time step alongside  $\tilde{e}_e$  modification to output temperature and  $\langle P \rangle$ . The results of the 1D mixing model are validated using 2D FLASH simulations.

### III. Validation of the model implemented in 1D Lagrangian framework

Distributions of  $\langle \rho \rangle$  and  $\tilde{e}_e$  for laser-ablated planar targets, obtained using the mixing model implemented in MULTI-IFE[39], are presented in Fig. 3(a) and (b). Solid lines represent FLASH simulations, while dashed lines correspond to MULTI-IFE simulations. Blue lines denote simulations with initial velocity perturbations, whereas red lines indicate simulations without perturbations. The overlapping red lines indicate that both simulations exhibit similar time evolution of  $\langle \rho \rangle$  and  $\tilde{e}_e$  despite differences in calculation cells. In the presence of perturbations, 2D simulations observe an increase in  $\tilde{e}_e$  and a decrease in  $\langle \rho \rangle$  near the bubble front; conversely,  $\tilde{e}_e$  decreases while  $\langle \rho \rangle$  increases near the spike front. Notably, the maximum specific internal energy gradient of electrons near the ablation front shifts outward toward the



coronal region due to mixing. The 1D mixing model accurately captures these characteristics except a larger deviation near the spike front, which is anticipated due to the higher difference of  $\tilde{e}_e$  between the initial and final states near the spike front, as shown in Fig. 2.

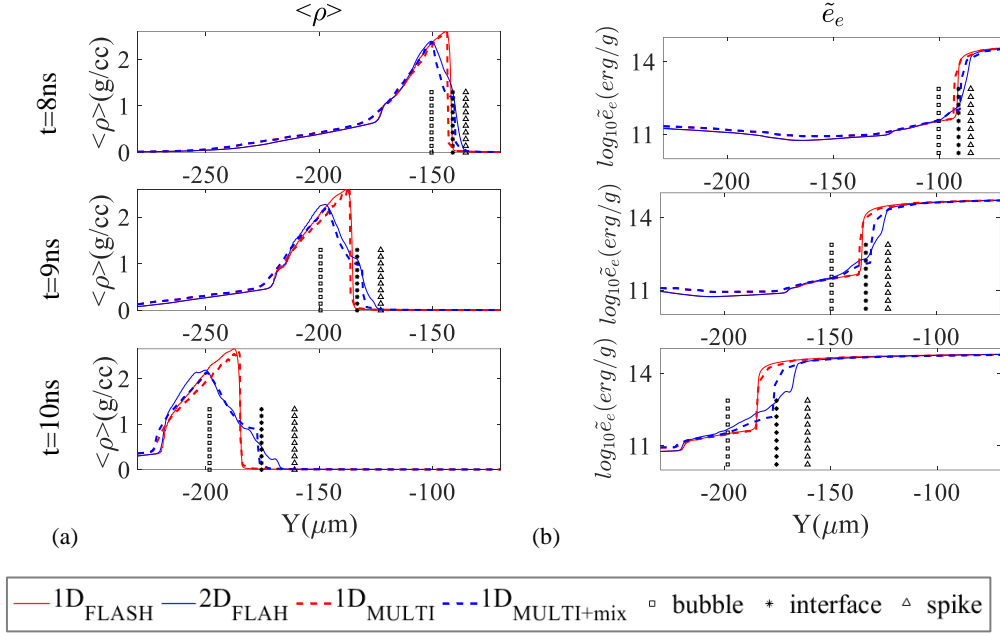


Fig. 3. Distributions of  $\langle \rho \rangle$  and  $\tilde{e}_e$  for cases with (blue) and without (red) velocity perturbations. The dashed line is calculated using MULTI-IFE.

We further quantify the influence of ARTI on the implosion shell, defined as the region between the internal and external points where the density equals  $1/e$  of the maximum density. At  $t = 10$  ns, the compression of the implosion shell, represented by the average density in planar geometry and mass-weighted adiabat, decreases by approximately 50% when mixing is considered. At this moment, the average density and mass-weighted adiabat of the implosion shell from 2D FLASH simulations, are 1.58 g/cc and 1.77, respectively, compared to 1.49 g/cc and 1.62 predicted by 1D MULTI-IFE. The relative errors for average density (5.7%) and mass-weighted adiabat

(8.5%) both remain below 10%, an acceptable limit. Furthermore,  $f$  in the expression of  $ME$  is relatively fixed, with  $f$  equal to 0.03, indicating that chunk mixing dominates. This stable value of  $f$  suggests that with knowledge of the evolution of  $h_B$  and  $v_B$ , one can effectively predict the evolution of the mean field.

#### IV. Application of the model to spherical implosion

As achieving high implosion quality in planar geometry is not feasible, we investigate the impact of reduced compression on implosion quality in spherical geometry. Different from planar geometry, the final state of internal energy in spherical geometry is calculated using  $\int_R 4\pi R^2 \langle \rho \rangle \tilde{e}_{e,ini} dR = \int_R 4\pi R^2 \langle \rho \rangle \tilde{e}_{e,fin} dR$ . Fig. 4 presents the pulse shape and streamline diagram for a 1.5-MJ triple-picket design [40] without the mixing model. The typical target scheme is color coded: the outer plastic has a density of 1g/cc, the middle DT ice has a density of 0.25g/cc, and the inner DT gas has a density of 3mg/cc. The inflight shell begins to accelerate at  $t = 5.5$  ns until the main shock reflects from the center to the interior of the inflight shell at  $t = 10.5$  ns, marking the onset of the deceleration phase. At approximately 11 ns, the hot spot stagnates, characterized by its minimum volume.

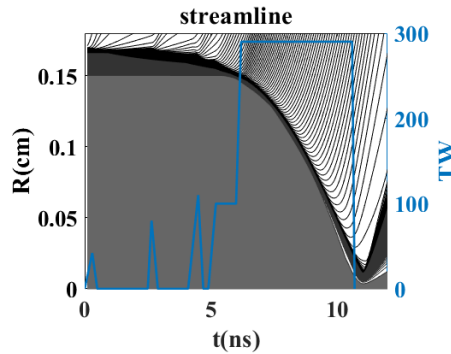


Fig. 4. Pulse shape and streamline diagram for a 1.5-MJ triple-picket design.

During the acceleration phase from 5.5 ns to 10.5 ns, we employ the mixing model at the ablation front with  $f = 0.03$ . We first compare the streamlines in the hot spot for cases without and with mixing. Fig. 5(a) and (b) demonstrate that, following the convergence of the main shock, a reflective shock wave, indicated by a green cycle, arises from the collision between the outer imploding DT gas and the inner exploding DT gas. The influence of mixing advances the onset of this reflected shock for a higher imploding velocity of DT gas. Additionally, due to the asynchronous deceleration of the flight shell and hot spot, the onset of deceleration, marked by a shock wave, advances with the influence of mixing. Furthermore, the stagnation, represented by a red dot, occurs earlier due to the prolonged influence of reduced compression.

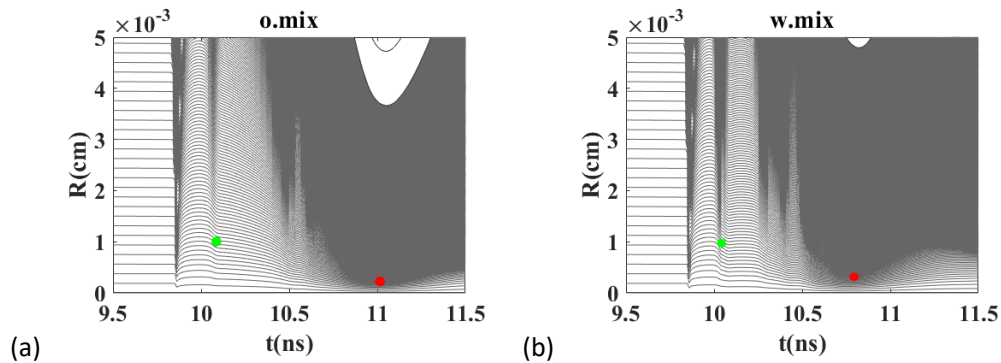


Fig. 5. Streamline diagrams for cases (a) without mixing and (b) with mixing. These characteristic moments denoted by dots are advance due to mixing.

Similar to planar cases, Fig. 6(a) shows that the mixing model results in a smaller inner radius [8] and an increased thickness of the inflight shell, indicating reduced compression. Fig. 6(d) reveals that mixing does not affect the convergence time of the main shock as it occurs with only minor perturbations at the onset of acceleration. The smaller inner radius of the inflight shell due to mixing leads to an earlier onset of the deceleration phase, as depicted in Fig. 6(b) and (e). This reduced radius, combined with

spherical geometry, results in higher density and pressure in the hot spot. At stagnation, the hot spot exhibit lower density and pressure with mixing. Fig. 6(c) and (f) also illustrate that while the case without mixing just reaches stagnation, the mixing case has already begun to expand. These phenomena suggest that the reduced compression associated with mixing may contribute to an earlier bang time [41, 42], which approaches stagnation.

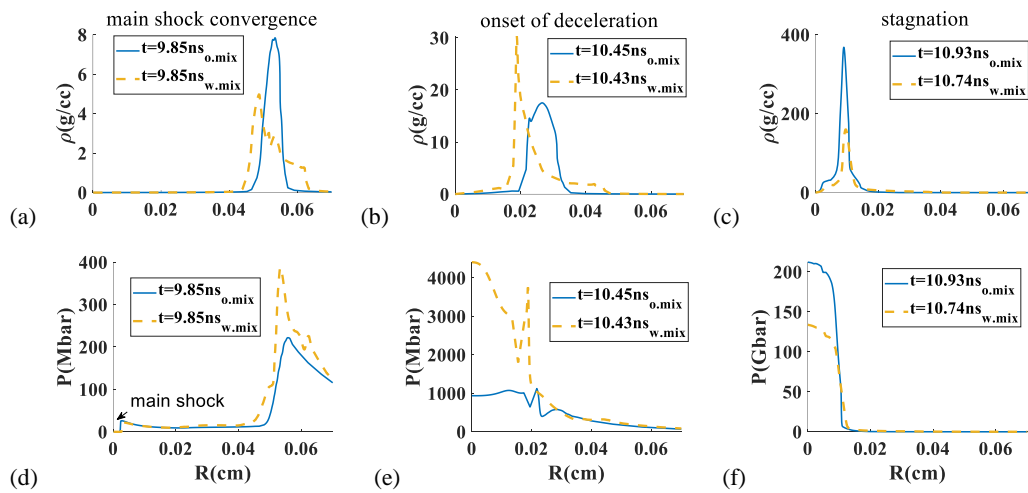


Fig. 6. Spatial distributions of density and pressure at three moments: the convergence of the main shock in (a) and (d), the end of the acceleration phase in (b) and (e), and the stagnation of the hot spot in (c) and (f). The hot spot density and stagnation pressure are both reduced due to mixing.

To guide the experiment measurements of self-emissivity, we present the total bremsstrahlung energy of the hot spot within a radius of 10 $\mu\text{m}$  in Fig. 7. The sharp rise in the self-emissivity signal, indicating the convergence of the main shock, remains consistent in both cases. While the reflective shock signal is unclear, the interval between the convergence of the main shock and stagnation is reduced, suggesting a potentially measurable signal in a single shot.

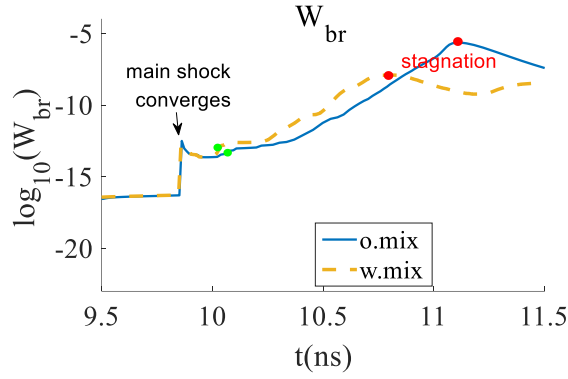


Fig. 7. The total bremsstrahlung energy of the hot spot within a radius of 10 $\mu$ m. The interval between the convergence of the main shock and stagnation is reduced under the influence of mixing.

## V. Conclusions

To address the challenges of high-dimensional and high-precision simulations, we propose a one-dimensional mixing model to investigate the impact of nonlinear ARTI on the compression of inflight shells. The mixing model modifies  $\tilde{\epsilon}$  in the mixed region by interpolating between an initial state of no mixing and a final state of isothermal molecular mixing. The interpolation depends on  $ME$ , characterized as a time-varying function of  $K_f / \tilde{E}_k$ , which includes a constant ranging from dominant chunk mixing ( $f \approx 0$ ) to dominant atomic mixing ( $f \approx 1$ ). After validation through two-dimensional simulations, the model was implemented in a Lagrangian framework, successfully capturing an increase in  $\tilde{\epsilon}$  and a decrease in  $\langle \rho \rangle$  near the bubble front, as well as a shift of the ablation front towards the coronal region. When applied to spherical implosion simulations, the mixing model suggests that a reduced time interval between the main shock convergence and the stagnation could yield a measurable signal in a single shot. Currently, the National Ignition Facility is focused on effectively mitigating mixing between high-Z ablaters and hot fuel, as well as low-mode drive asymmetry, to enhance target gain. We are optimistic that successfully addressing these

critical issues will prioritize increasing compression in the future. Overall, this model serves as a valuable tool for investigating the impact of ARTI, and other hydrodynamic instabilities if it is appropriately modified.

### **Acknowledgments**

This work is supported by the supported by the National Key R & D Projects (Grant No. 2023YFA1608402), Strategic Priority Research Program of the Chinese Academy of Sciences (Grant No. XDA25010200), and Nature Science Foundation of China (Grant No. 12375242).

### **References**

- [1] Abu-Shawareb, H., Acree, R., Adams, P., Adams, J., Addis, B., Aden, R., Adrian, P., Afeyan, B. B., Aggleton, M., Aghaian, L., ... and Zylstra, A. B., 2022. Lawson criterion for ignition exceeded in an inertial fusion experiment. *Physical Review Letters*, 129(7), p.075001.
- [2] Abu-Shawareb, H., Acree, R., Adams, P., Adams, J., Addis, B., Aden, R., Adrian, P., Afeyan, B. B., Aggleton, M., Aghaian, L., ... and Zylstra, A. B., 2024. Achievement of target gain larger than unity in an inertial fusion experiment. *Physical Review Letters*, 132(6), p.065102.
- [3] Hurricane, O. A., Patel, P. K., Betti, R., Froula, D. H., Regan, S. P., Slutz, S. A., Gomez, M. R. and Sweeney, M. A., 2023. Physics principles of inertial confinement fusion and US program overview. *Reviews of Modern Physics*, 95(2), p.025005.
- [4] Nuckolls, J., Wood, L., Thiessen, A. and Zimmerman, G., 1972. Laser compression of matter to super-high densities: Thermonuclear (CTR) applications. *Nature*, 239(5368), pp.139-142.
- [5] Theobald, W., Solodov, A. A., Stoeckl, C., Anderson, K. S., Beg, F. N., Epstein, R., Fiksel, G., Giraldez, E. M., Glebov, V. Y., Habara, H., ... and Wei, M. S., 2014. Time-resolved compression of a capsule with a cone to high density for fast-ignition laser fusion. *Nature*

*Communications*, 5(1), p.5785.

- [6] Robey, H. F., MacGowan, B. J., Landen, O. L., LaFortune, K. N., Widmayer, C., Celliers, P. M., Moody, J. D., Ross, J. S., Ralph, J., LePape, S., ... and Edwards, M. J., 2013. The effect of laser pulse shape variations on the adiabat of NIF capsule implosions. *Physics of Plasmas*, 20(5), p.052707.
- [7] Kritcher, A. L., Zylstra, A. B., Callahan, D. A., Hurricane, O. A., Weber, C. R., Clark, D. S., Young, C. V., Ralph, J. E., Casey, D. T., Pak, A., ... and Zimmerman, G. B., 2022. Design of an inertial fusion experiment exceeding the Lawson criterion for ignition. *Physical Review E*, 106(2), p.025201.
- [8] Michel, D. T., Hu, S. X., Davis, A. K., Glebov, V. Y., Goncharov, V. N., Igumenshchev, I. V., Radha, P. B., Stoeckl, C. and Froula, D. H., 2017. Measurement of the shell decompression in direct-drive inertial-confinement-fusion implosions. *Physical Review E*, 95(5), p.051202.
- [9] Liu, D. X., Tao, T., Li, J., Jia, Q. and Zheng, J., 2022. Mitigating laser imprint with a foam overcoating. *Physics of Plasmas*, 29(7), p.072707.
- [10] Johnson, M. G., Frenje, J. A., Casey, D. T., Li, C. K., Séguin, F. H., Petrasso, R., Ashabranner, R., Bionta, R. M., Bleuel, D. L., Bond, E. J., ... and Nelson, A. J., 2012. Neutron spectrometry—An essential tool for diagnosing implosions at the National Ignition Facility. *Review of Scientific Instruments*, 83(10), p.10D308.
- [11] Frenje, J. A., Bionta, R., Bond, E. J., Caggiano, J. A., Casey, D. T., Cerjan, C., Edwards, J., Eckart, M., Fittinghoff, D. N., Friedrich, S., ... and Wilson, D. C., 2013. Diagnosing implosion performance at the National Ignition Facility (NIF) by means of neutron spectrometry. *Nuclear Fusion*, 53(4), p.043014.

- [12] Landen, O. L., Casey, D. T., DiNicola, J. M., Doeppner, T., Hartouni, E. P., Hinkel, D. E., Hopkins, L. B., Hohenberger, M., Kritcher, A. L., LePape, S., ... and Weber, C. R., 2020. Yield and compression trends and reproducibility at NIF. *High Energy Density Physics*, 36, p.100755.
- [13] Thomas, C. A., Campbell, E. M., Baker, K. L., Casey, D. T., Hohenberger, M., Kritcher, A. L., Spears, B. K., Khan, S. F., Nora, R., Woods, D. T., ... and Finnegan, S. M., 2020. Deficiencies in compression and yield in x-ray-driven implosions. *Physics of Plasmas*, 27(11), p.112705.
- [14] Meaney, K. D., Kim, Y. H., Geppert-Kleinrath, H., Herrmann, H. W., Hopkins, L. B. and Hoffman, N. M., 2020. Diagnostic signature of the compressibility of the inertial-confinement-fusion pusher. *Physical Review E*, 101(2), p.023208.
- [15] Scott, R. H. H., Clark, D. S., Bradley, D. K., Callahan, D. A., Edwards, M. J., Haan, S. W., Jones, O. S., Spears, B. K., Marinak, M. M., Town, R. P. J., ... and Suter, L. J., 2013. Numerical modeling of the sensitivity of X-ray driven implosions to low-mode flux asymmetries. *Physical Review Letters*, 110(7), p.075001.
- [16] Rinderknecht, H. G., Casey, D. T., Hatarik, R., Bionta, R. M., MacGowan, B. J., Patel, P., Landen, O. L., Hartouni, E. P. and Hurricane, O. A., 2020. Azimuthal drive asymmetry in inertial confinement fusion implosions on the National Ignition Facility. *Physical Review Letters*, 124(14), p.145002.
- [17] Edgell, D. H., Radha, P. B., Katz, J., Shvydky, A., Turnbull, D. and Froula, D. H., 2021. Nonuniform absorption and scattered light in direct-drive implosions driven by polarization smoothing. *Physical Review Letters*, 127(7), p.075001.
- [18] Kritcher, A. L., Ralph, J., Hinkel, D. E., Döppner, T., Millot, M., Mariscal, D., Benedetti, R., Strozzi, D. J., Chapman, T., Goyon, C., ... and Hurricane, O. A. (2018). Energy transfer



between lasers in low-gas-fill-density hohlraums. *Physical Review E*, 98(5), 053206.

- [19] Li, J., Yan, R., Zhao, B., Zheng, J., Zhang, H. and Lu, X., 2022. Mitigation of the ablative Rayleigh–Taylor instability by nonlocal electron heat transport. *Matter and Radiation at Extremes*, 7(5), p.055902.
- [20] Li, J., Yan, R., Zhao, B., Wu, J., Wang, L. and Zou, S., 2024. Effect of hot-electron preheating on the multimode bubble-front growth of the ablative Rayleigh–Taylor instability. *Physics of Plasmas*, 31(1), p.012703.
- [21] Jones, O. S., Suter, L. J., Scott, H. A., Barrios, M. A., Farmer, W. A., Hansen, S. B., Liedahl, D. A., Mauche, C. W., Moore, A. S., Rosen, M. D., ... and Turnbull, D. P., 2017. Progress towards a more predictive model for hohlraum radiation drive and symmetry. *Physics of Plasmas*, 24(5), p.056312.
- [22] Robey, H. F., Boehly, T. R., Celliers, P. M., Eggert, J. H., Hicks, D., Smith, R. F., Collins, R., Bowers, M. W., Krauter, K. G., Datte, P. S., ... and Moses, E., 2012. Shock timing experiments on the National Ignition Facility: initial results and comparison with simulation. *Physics of Plasmas*, 19(4), p.042706.
- [23] Cheng, B., Kwan, T. J., Wang, Y. M., Yi, S. A., Batha, S. H. and Wysocki, F. J., 2016. Effects of preheat and mix on the fuel adiabat of an imploding capsule. *Physics of Plasmas*, 23(12), p.120702.
- [24] Amendt, P., 2021. Entropy generation from hydrodynamic mixing in inertial confinement fusion indirect-drive targets. *Physics of Plasmas*, 28(7), p.072701.
- [25] Pak, A. (2023). Overview of principal degradations arising from capsule target perturbations in inertial confinement fusion implosions (No. LLNL-CONF-854535). Lawrence Livermore

National Laboratory (LLNL), Livermore, CA (United States).

- [26] Divol, L., Pak, A., Bachmann, B., Baker, K. L., Baxamusa, S., Biener, J., and Wilde, C. H. 2024. Thermonuclear performance variability near ignition at the National Ignition Facility. *Physics of Plasmas*, 31(10), p.102703
- [27] Goncharov, V. N., Gotchev, O. V., Vianello, E., Boehly, T. R., Knauer, J. P., McKenty, P. W., Cherfils-Cl  rouin, C. (2006). Early stage of implosion in inertial confinement fusion: Shock timing and perturbation evolution. *Physics of plasmas*, 13(1), p.012702.
- [28] Liu, D. X., Tao, T., Li, J., Jia, Q. and Zheng, J., 2022. Mitigating laser imprint with a foam overcoating. *Physics of Plasmas*, 29(7), p.072707.
- [29] Clark, D. S., Weber, C. R., Milovich, J. L., Pak, A. E., Casey, D. T., Hammel, B. A., Ho, D. D., Jones, O. S., Koning, J. M., Kritcher, A. L., ... and Edwards, M. J., 2019. Three-dimensional modeling and hydrodynamic scaling of National Ignition Facility implosions. *Physics of Plasmas*, 26(5), p050601.
- [30] Clark, D. S., Weber, C. R., Milovich, J. L., Salmonson, J. D., Kritcher, A.L., Haan, S. W., Hammel, B. A., Hinkel, D. E., Hurricane, O. A., Jones, O. S., ... and Edwards, M. J., 2016. Three-dimensional simulations of low foot and high foot implosion experiments on the National Ignition Facility. *Physics of Plasmas*, 23(5), p056302.
- [31] Welser-Sherrill, L., Cooley, J. H., Haynes, D. A., Wilson, D. C., Sherrill, M. E., Mancini, R. C., and Tommasini, R., 2008. Application of fall-line mix models to understand degraded yield. *Physics of Plasmas*, 15(7), p.072702.
- [32] Bachmann, B., MacLaren, S. A., Bhandarkar, S., Briggs, T., Casey, D., Divol, L., D  ppner, T., Fittinghoff, D., Freeman, M., Haan, S., ... and Wray, A., 2022. Measurement of dark ice-

- ablator mix in inertial confinement fusion. *Physical Review Letters*, 129(27), p.275001.
- [33] Bachmann, B., MacLaren, S. A., Masse, L., Bhandarkar, S., Briggs, T., Casey, D., Divol, L., Döppner, T., Fittinghoff, D., Freeman, M., ... and Wray, A., 2023. Measuring and simulating ice–ablator mix in inertial confinement fusion. *Physics of Plasmas*, 30(5), p.052704.
- [34] Xiao, M., Zhang, Y. and Tian, B., 2020. Modeling of turbulent mixing with an improved K–L model. *Physics of Fluids*, 32(9), p.092104.
- [35] Morgan, B. E., 2022. Simulation and Reynolds-averaged Navier-Stokes modeling of a three-component Rayleigh-Taylor mixing problem with thermonuclear burn. *Physical Review E*, 105(4), p.045104.
- [36] Dimonte, G., 2000. Spanwise homogeneous buoyancy-drag model for Rayleigh–Taylor mixing and experimental evaluation. *Physics of plasmas*, 7(6), pp.2255-2269.
- [37] Liu, D. X., Tao, T., Li, J., Jia, Q., Yan, R., Zheng, J., 2024, Extended buoyancy-drag model for ablative Rayleigh-Taylor instability seeded by various perturbations, arXiv:2411.12392.
- [38] Fryxell, B., Olson, K., Ricker, P., Timmes, F. X., Zingale, M., Lamb, D. Q., MacNeice, P., Rosner, R., Truran, J. W. and Tufo, H., 2000. FLASH: An adaptive mesh hydrodynamics code for modeling astrophysical thermonuclear flashes. *The Astrophysical Journal Supplement Series*, 131(1), p.273.
- [39] Ramis, R. and Meyer-ter-Vehn, J., 2016. MULTI-IFE—A one-dimensional computer code for Inertial Fusion Energy (IFE) target simulations. *Computer Physics Communications*, 203, pp.226-237.
- [40] Craxton, R. S., Anderson, K. S., Boehly, T. R., Goncharov, V. N., Harding, D. R., Knauer, J. P., McCrory, R. L., McKenty, P. W., Meyerhofer, D. D., Myatt, J. F., ... and Zuegel, J. D. (2015).

Direct-drive inertial confinement fusion: a review. *Physics of Plasmas*, 22(11), p.110501.

[41] Rygg, J.R., Frenje, J. A., Li, C. K., Seguin, F. H., Petrasso, R. D., Glebov, V. Yu, Meyerhofer, D. D., Sangster, T. C., and Stoeckl, C. 2007. Time-dependent nuclear measurements of mix in inertial confinement fusion. *Physical Review Letters*, 98(21), p.215002.

[42] Robey, H. F., Smalyuk, V. A., Milovich, J. L., Döppner, T., Casey, D. T., Baker, K. L., Peterson, J. L., Bachmann, B., Berzak Hopkins, L. F., Bond, E., ... and Gatu Johnson, M. 2016. Performance of indirectly driven capsule implosions on the national ignition facility using adiabat-shaping. *Physics of Plasmas*, 23(5), p.056303.